Proceedings of the
4th JSME-KSME Thermal Engineering Conference
October 1-6, 2000, Kobe Japan

F311

HEAT AND MOMENTUM TRANSFER IN ROTATING TURBULENT CHANNEL FLOW

O. El-Samni* and N. Kasagi*

***Department of Mechanical Engineering, The University of Tokyo, Hongo 7-3-1, Bunkyo-ku, Tokyo 113-8656, Japan**

ABSTRACT The transport of mass and heat in turbulent flows is of great importance in the field of turbomachinery and also in many other industrial applications. Understanding the heat transfer mechanism near the wall of rotating passages should be essential if more advanced temperature control is to be applied in order to increase the efficiency of turbomachines. Direct numerical simulation of the fully developed thermal field in a turbulent channel flow subjected to system rotation has been performed using a spectral method. Two axes of rotation in the spanwise and streamwise directions are to be examined. Constant, but different wall temperatures are assumed on the two walls. The rotation number is increased to 15. The mean quantities, flow and thermal turbulence statistics, and heat fluxes are presented and discussed. The streamwise rotation causes continuous enhancement of heat transfer with increasing the rotation rate, while a rotation number around 7.5 gives the optimum enhancement in the case of spanwise rotation.

Keywords: Turbulent heat transfer, system rotation, channel flow, DNS.

INTRODUCTION

The flow inside turbomachinery has complicated nature due to the interaction between Coriolis, centrifugal, buoyancy forces arising with the rotation and curvature of the passages. In addition to conventional large-scale gas turbines, developments of highly efficient gas turbines of micro-to-small scales are now going on because of their reliability, compactness, higher efficiencies, and less effluence. The basic concept is to attain higher levels of temperatures. New materials to withstand high temperatures and new technologies for turbine blade cooling are now under development. Clear understanding of the mechanism of heat transfer near the wall in rotating ducts is needed in order to design efficient and reliable gas turbines. Direct numerical simulation (hereafter DNS) becomes a valuable tool, which can produce detailed information about the instantaneous flow and temperature fields for simple configuration problems. Turbulence modelers have used databases generated from DNS to assess the turbulence models, in which system rotation effect is incorporated. This, in turns, will improve the performance of CFD packages, which are considered the appropriate tool in designing gas turbines with less computational cost and high predictability of flow behaviour.

Turbulent channel flow subjected to system rotation has been studied experimentally and numerically for more than four decades since the experimental work of Johnston et al. [1]. Johnston and his co-workers observed the stabilization of turbulent flow near the leading (suction) wall and the augmentation of turbulence near the trailing (pressure) wall in a spanwise rotating channel. Kim [2] used LES to study the effect of spanwise rotation at a Reynolds number of 13800, which is based on the centerline velocity and the channel half width, and reproduced most of the observations in the experiments. Kristoffersen and Andersson [3] also used DNS to study the effect of spanwise rotation using a finite difference algorithm with rotation numbers up to 7.6, based on the friction velocity. Andersson and Kristoffersen [4] provided detailed turbulence statistics from their earlier databases [3]. Recently, Oberlack et al. [5] studied streamwise system rotation using DNS, LES and turbulence models. They observed some similarity to the classical spanwise rotation case and found characteristic induction of the mean spanwise velocity component. Non-zero Reynolds stresses were also recognized. The rotation numbers of 3.2 and 10 were tested in their simulations.

The transport of scalar in turbulent channel flow was studied mainly for different Prandtl numbers [6-8]. Nishimura and Kasagi [9] studied the combined effect of system rotation and buoyancy, concluding a highly complicated nature of flow and temperature fields according to the orientation of both body forces. There is, however, a lack of general knowledge about system rotation effect on scalar transport.

The present work aims at studying the effect of system rotation on the temperature field assuming the temperature as a passive scalar with no buoyancy. Two cases will be discussed: the spanwise and streamwise rotating channels, while extending the rotation number up to 15.0, which has not been studied before.

NUMERICAL FORMULATION

The fully developed turbulent channel flow driven by a constant pressure gradient is assumed with the homogeneity in the streamwise x and spanwise z directions. Two different temperatures at the two walls are assumed constant with no buoyancy forces. The Prandtl number Pr is kept constant at 0.71, which corresponds to most of working fluids in gas turbines. The flow geometry is shown in Fig. 1.

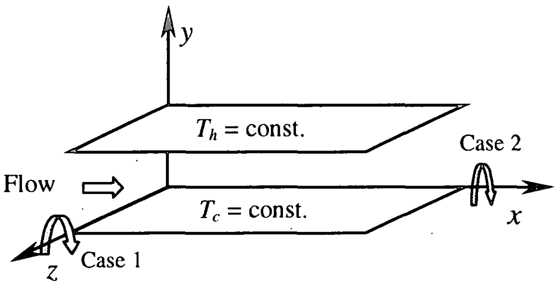

Figure 1 Flow Geometry.

The present DNS used $64 \times 65 \times 64$ grid points with a domain size of $5\pi\delta \times 2\delta \times 2\pi\delta$ in the streamwise, wall-normal and spanwise directions, respectively. The variables have been non-dimensionalized by the channel half width δ, friction velocity u_τ and temperature difference ΔT. The corresponding dimensionless parameters in the present study are the rotation number:

$$Ro_\tau = 2\delta\Omega / u_\tau , \tag{1}$$

and the Reynolds number:

$$Re_\tau = \delta u_\tau / \nu . \tag{2}$$

The simulations are extended to higher rotation numbers up to 15.0, which is nearly twice as large as the rotation number in Kristoffersen and Andersson [3]. The present study is concerned with the effect of spanwise (case I) and streamwise (case II) rotation on the flow and thermal fields. A spectral method with Fourier expansion in the homogeneous directions x and z, and Chebyshev polynomials in the wall-normal direction are used. Refer to Kasagi and Iida [6, 10] for more details about the numerical technique. The Reynolds and Prandtl numbers are fixed at 150 and 0.71, respectively. The two walls are kept at two different temperatures, by which the scalar is transferred from the hot to cold walls. The integration extends at each rotation number with a time step of $0.12\,\nu/u_\tau^2$ until the flow field reaches a fully developed state and the average total heat flux becomes constant at any distance from the wall. Then, the integration continues for $4800\,\nu/u_\tau^2$ in order to calculate turbulence statistics.

RESULTS AND DISCUSSIONS

Spanwise Rotation (Case I)

The Nusselt number and friction coefficient, normalized by their corresponding non-rotating values, are plotted in Fig. 2. Good agreement with data of Kristoffersen and Andersson [3] is noticed for the skin friction coefficient. For the rotation number of 7.5, both Nu and C_f reach their maxima for the range studied. For Ro_τ higher than 7.5, the two parameters gradually decrease on both walls.

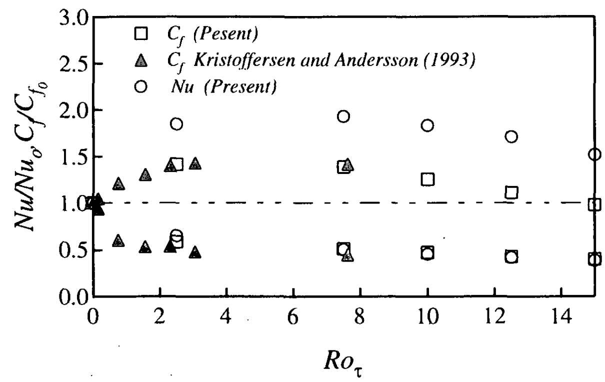

Figure 2 Nusselt number and friction coefficient (Case I)

The mean velocity profiles for different rotation numbers are shown in Fig. 3(a), in which the linear regimes are clearly evident at higher rotation number with wider depth and a slope of 2Ω. The stabilization process occurs at the suction side, and a highly turbulent flow can be observed near the pressure side with a slight increase in the bulk mean velocity U_m. The mean temperature profiles, shown in Fig. 3(b), are to some extent correlated to the mean streamwise velocity and show the increased and decreased temperature drops near the suction and pressure sides, respectively.

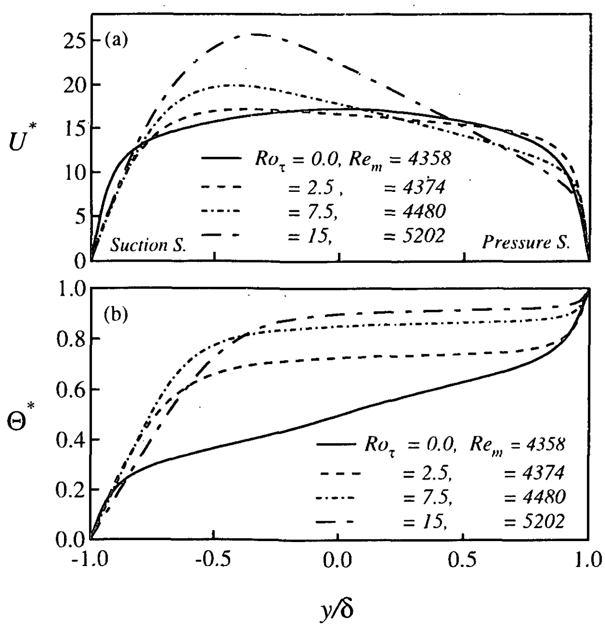

Figure 3; Mean profiles of; (a) streamwise velocity, (b) mean temperature (Case I).

The wall-units plots of mean temperatures normalized by the friction temperature θ_τ are shown in Fig. 4, in which the solid line corresponds to the non-rotation case. Two distinguished features can be observed on both sides of the channel.

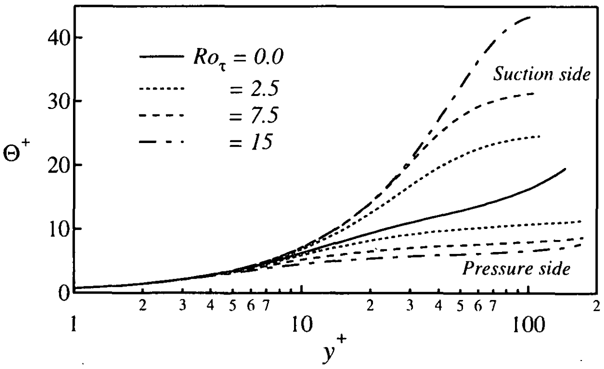

Figure 4 Temperature profiles in wall units (Case I).

The turbulence intensities generated in the spanwise rotating channel, have been confirmed to have similar trends as those in medium rotation number simulations [3, 4] (not shown here) and the suppression of the normal stress $\overline{uu}$ near the pressure side is well captured for $Ro_\tau \geq 2.5$. The focus will be on the pressure side in the coming figures. For all range of rotation numbers, $\overline{vv}$ and $\overline{ww}$ stresses, on the other hand, show continuous enhancement over two thirds of the channel width near the pressure side. The stress anisotropy ($\overline{uu} - \overline{vv}$) reduces consequently. A similarity between the streamwise velocity component and temperature is observed in Fig. 5. In the vicinity of the pressure side ($y^+ \leq 10$), the rms fluctuations of u and θ are highly correlated. Their peak values become closer to the wall with slight decrement as the rotation number increases.

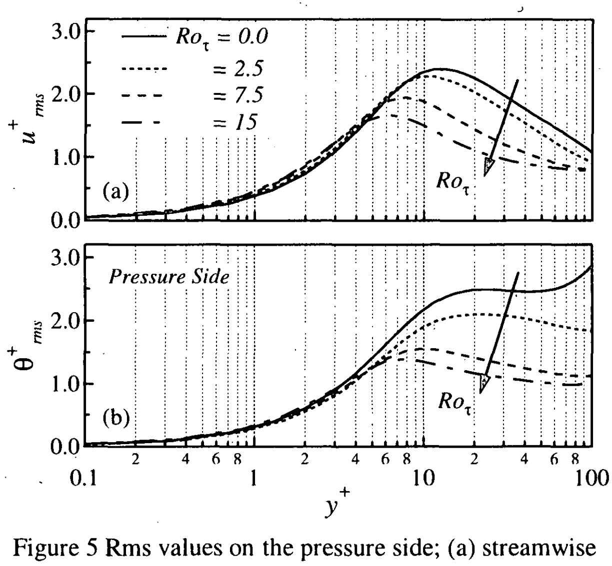

Figure 5 Rms values on the pressure side; (a) streamwise velocity; (b) temperature (Case I).

Figure 6 shows the three components of vorticity variance ω^2. In the vicinity of the wall, both ω_z^2 and ω_x^2 increase with increasing rotation number, and ω_x^2 exceeds drastically ω_z^2. The streamwise component ω_x^2 becomes larger than ω_z^2 and ω_y^2 components at $y^+ \geq 10$ where the later two components are nearly equal. Large-scale streamwise vortices were observed in low-rotation number simulations closer to the pressure side [9].

Figure 7(a) shows the decrement of streamwise heat flux with increasing the rotation. The trend is much similar to the observations in Fig. 5(a, b). The wall-normal heat flux is enhanced more significantly near the wall as shown in Fig. 7(b). The production terms of wall-normal heat flux are plotted in Fig. 8. The blank symbols correspond to the rotational production term $G_{j\theta}$, which becomes nearly twice the mean gradient production and its peak shifts towards to the wall. This is the reason for the enhancement the wall-normal heat flux in the vicinity of the pressure side.

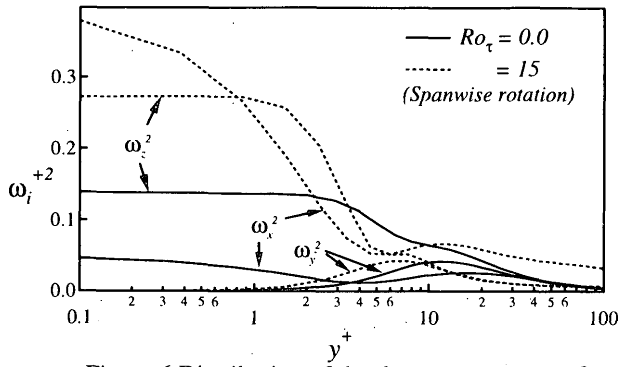

Figure 6 Distribution of the three components of vorticity variance (Case I).

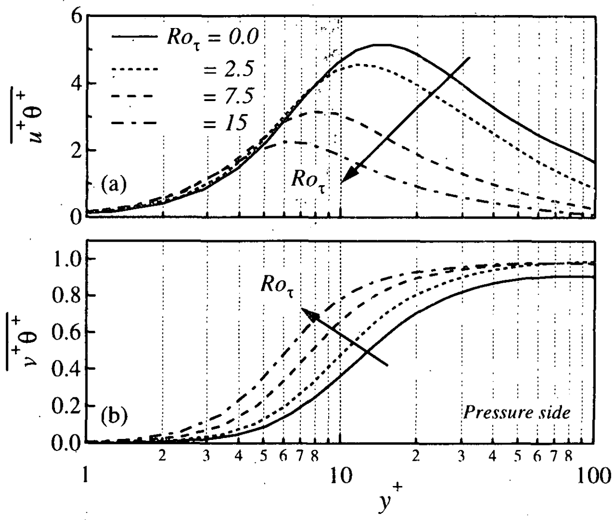

Figure 7 Turbulent heat fluxes; (a) streamwise, (b) wall-normal heat fluxes (Case I).

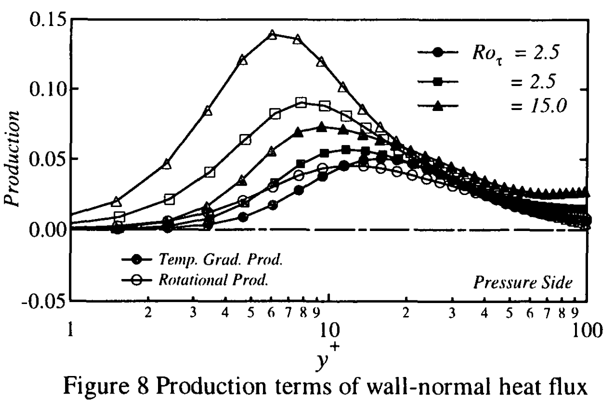

Figure 8 Production terms of wall-normal heat flux (Case I).

Streamwise Rotation (Case II)

Unlike the spanwise rotation case, the Nusselt number and friction coefficient in the streamwise rotation case increase monotonously with increasing the rotation number as shown in Fig. 9. It may be worthy to mention those coefficients are symmetry at the two walls in this case.

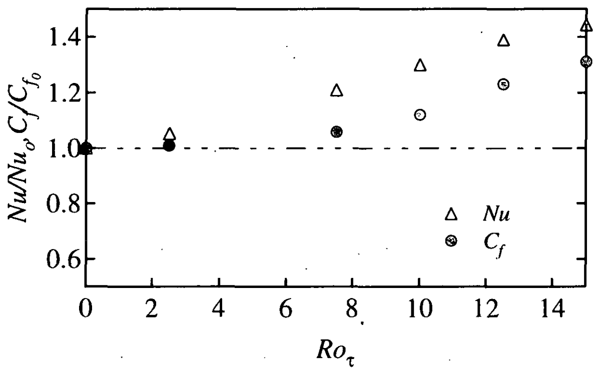

Figure 9 Nusselt number and friction coefficient (Case II).

In Fig. 10(a), the streamwise velocity component, unlike in case I, is symmetric with respect to the channel center and shows decrement in the mass flow rate. Two linear regimes emerge on both sides of channel centerline as predicted by Oberlack et al. [5]. The Coriolis forces in the streamwise rotating channel disturb the flow in the lateral directions and this results in a mean spanwise velocity component with anti-symmetric profiles around the centerline. As shown in Fig. 10(b), four typical regions of opposite motions are captured for all the rotation numbers studied. The peaks of spanwise mean velocity near the wall increase while increasing the rotation number more obvious than the local peaks near the channel center.

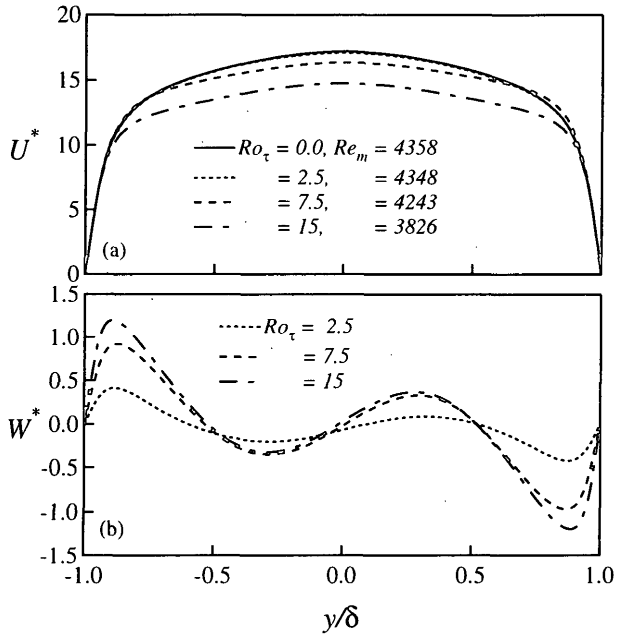

Figure 10 Mean velocity; (a) streamwise; and (b) spanwise components (Case II).

The mean temperature profiles are skewed around the channel centerline giving higher gradients near the walls, as shown in Fig. 11(a). Figure 11(b) shows the logarithmic trend of temperature similar to that of streamwise velocity at different rotation numbers; $\Theta^+ = 1/k_\theta \ln y^+ + C_\theta$. The von Kàrmàn coefficient k_θ changes between 0.27 and 0.645 at the lowest and the highest rotation numbers, respectively.

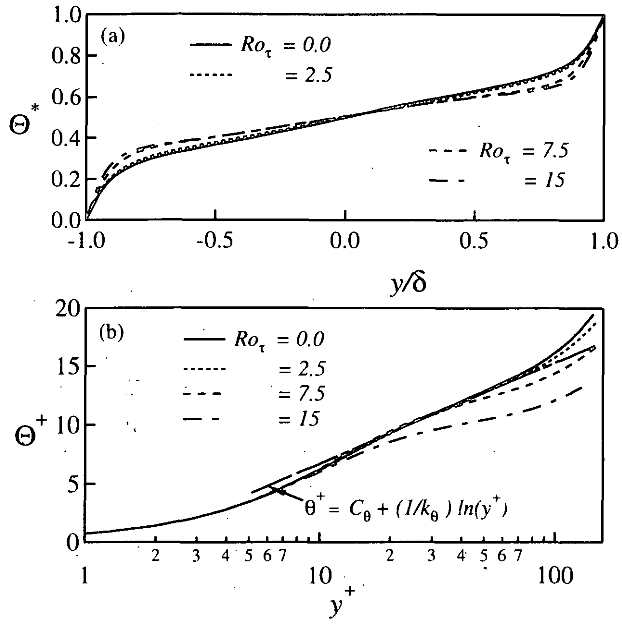

Figure 11 Mean temperature profiles; (a) along channel width; (b) in wall units (Case II).

The rms values of streamwise velocity and temperature fluctuations are activated slightly than the non-rotating case, as shown in Fig. 12. The augmentation of v_{rms} and w_{rms} components are recognized better at higher rotation numbers over the whole channel, but not shown here. The streamwise component u_{rms} slightly decreases near the wall at the higher rotation numbers; see Fig. 12 (a). The non-zero off-diagonal stresses and the gradient of spanwise mean velocity affect the generation of Reynolds stresses and heat fluxes as well.

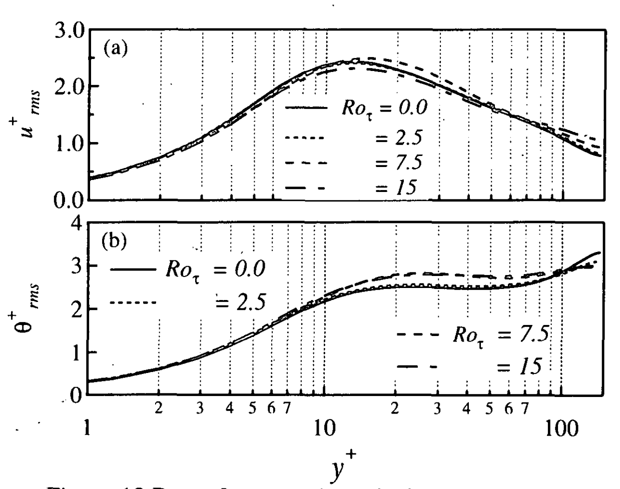

Figure 12 Rms of streamwise velocity and temperature fluctuations (Case II).

Figure 13 shows a general decrement the three components of vorticity variance far from the wall. Going closer to the wall, ω_z^2 decreases behind its corresponding non-rotating asymptotic value. On the other hand, the ω_x^2 component increases in the vicinity of the wall but unlike case I, it doesn't exceed ω_z^2.

At higher rotation, the streamwise heat flux, shown in Fig. 14(a), tends to decrease as a consequence of suppressed streamwise Reynolds stress. In Fig. 14(b), a tendency for suppression near the wall and then augmentation can be observed for the wall-normal heat flux with increasing the rotation number. A remarkable note here is the generation of the spanwise heat flux $\overline{w\theta}$, which shows high sensitivity to the system rotation with its maximum lies around $10 \le y^+ \le 20$ as shown in Fig. 14(c). The spanwise heat flux plays a direct role in enhancing the wall-normal flux again through the rotational production term.

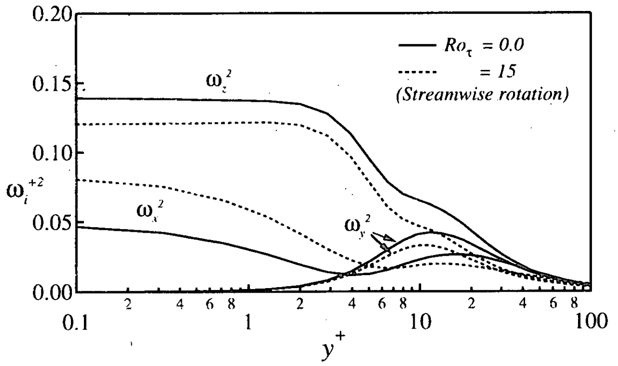

Figure 13 Distribution of vorticity components (Case II).

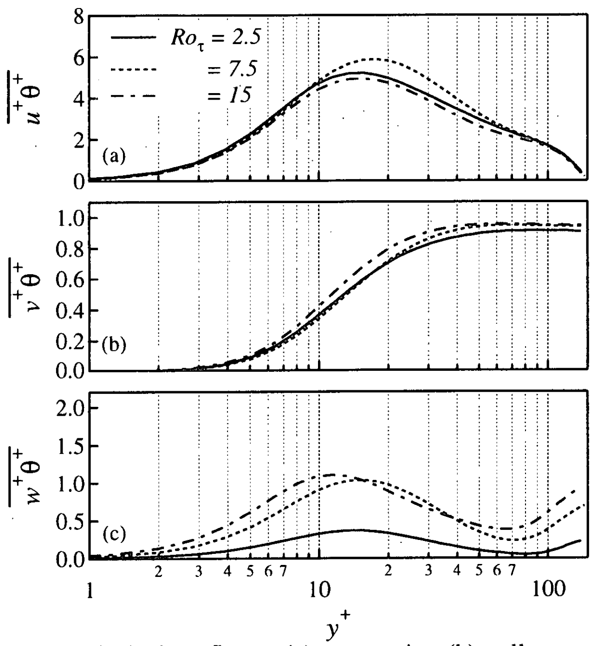

Figure 14 The heat fluxes; (a) streamwise, (b) wall-normal, (c) spanwise heat fluxes (Case II).

Figure 15(a) compares the rotational production terms to the mean gradient production (*MGP*) in streamwise rotating channel. At a lower rotation number, the rotation effect is negligible. With increasing the rotation, the, $G_{2\theta}$ becomes dominant in the near wall vicinity, whilst the mean gradient production decreases. The pressure-temperature correlation plays a basic role in destructing the wall-normal heat flux. For the newly generated flux $\overline{w\theta}$, the rotational production term, which depends directly on the wall-normal heat flux, becomes dominant with increasing the rotation as shown in Fig. 15(b).

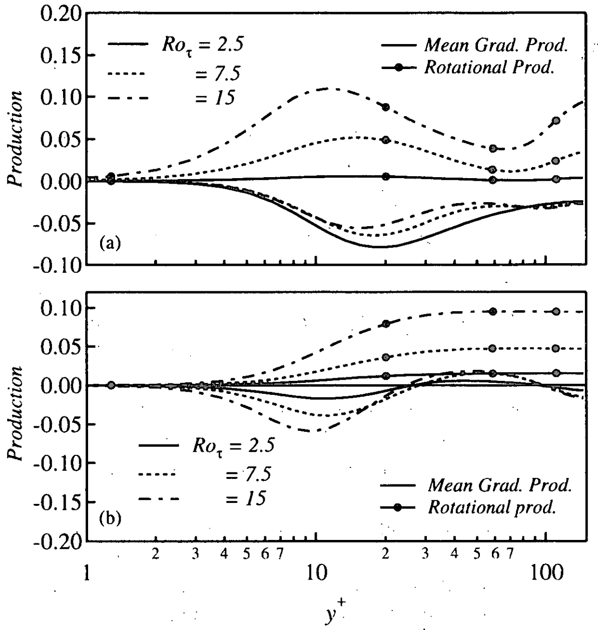

Figure 15 Production terms of heat fluxes; (a) wall-normal, (b) spanwise heat flux (Case II).

Conclusions

A series of DNS have been performed for higher rotation numbers in order to investigate the effect of system rotation on the scalar transport. Two basic orientation cases were studied; spanwise and streamwise rotating channel flow. The study demonstrates the significant enhancement of scalar transport. For a spanwise rotating channel, the rotation number of 7.5 seems to be optimum for maximizing the scalar transport, while the rotation number of 15 gives globally the same outcome of non-rotating case. The effect of rotation on the vortical structure differs in the two cases studied. While large vortices have been revealed in the spanwise rotation, the streamwise case shows elongated structure. The rotation affects directly the wall-normal heat flux through the additional rotational production, and indirectly through the Reynolds stresses and the mean gradients of streamwise velocity and temperature. In the streamwise rotation case, the turbulence is activated through the enhancement of all the normal stresses. The spanwise heat flux is generated and enhanced with increasing the rotation number in the buffer region.

This directly affects the production of wall-normal flux and augments the mechanism of scalar transport. Continuous increase in Nusselt number and friction coefficient is also observed while increasing the rotation number. The rate of increase of friction coefficient is less than that of Nusselt number; this fact is hardly observed in many other cases of convective heat transfer.

Acknowledgment

This numerical work is the results of "Micro Gas Turbine/Fuel Cell Hybrid-Type Distributed Energy System" which is supported by the Department of Core Research for Evolutional Science and Technology (CREST) in the Program of Japan Science and Technology Corporation (JST).

Nomenclature

C_f	friction coefficient, $C_f = 2\tau_w/\rho U_m^2$
c_p	specific heat at constant pressure
C_θ	constant
$G_{i\theta}$	Rotational production term, $= -2\varepsilon_{jkl}\,\Omega_k\,\overline{u_l\theta}$
k_θ	von Kàrmàn constant
MGP	mean gradient production term = $\overline{\theta u_k}\,\partial U_j/\partial x_k + \overline{u_j u_k}\,\partial\Theta/\partial x_k$
Nu	Nusselt number, $Nu = 2\delta q_w/(T_m - T_w)\lambda$
Pr	Prandtl number
q	heat flux
Re_m	Reynolds number, $Re = 2U_m\delta/\nu$
Re_τ	Reynolds number, $Re_\tau = u_\tau\delta/\nu$
Ro	Rotation number, $Ro = 2\delta\Omega/U_m$
Ro_τ	Rotation number, $Ro_\tau = 2\delta\Omega/u_\tau$
T	temperature in ^oC
T_h	temperature of the hot wall
T_c	temperature of the cold wall
T_τ	friction temperature on the wall $q_w/\rho c_p u_\tau$
U, W	mean velocities
u, v, w	fluctuating velocities
u_τ	friction velocity,
u_τ^*	friction velocity based on the shear averaged on the two walls.
x, y, z	streamwise, wall-normal, and spanwise coordinate systems

Greek symbols

ΔT	temperature difference ($T_h - T_c$)
δ	channel half width
λ	thermal conductivity.
ν	kinematic viscosity
Θ	mean temperature difference normalized by ΔT
θ	temperature fluctuation normalized by ΔT
τ	shear stress
Ω	angular velocity of rotation

Subscripts and superscripts

m	bulk-averaged
rms	root mean square value
p	normalized by the pressure wall value
s	normalized by the suction wall value
w	value at the wall
+	normalized by wall variables; u_τ, T_τ, and ν on each wall
*	normalized by u_τ^*
―	ensemble average over x-z plane and time

References

1. Johnson, J. P., Halleen, R. M. and Lezius, D. K., Effects Of Spanwise Rotation On The Structure Of Two-Dimensional Fully Developed Turbulent Channel Flow, J. Fluid Mech., Vol. 56, (1972), pp. 533-557.
2. Kim, J., The Effect Of Rotation on Turbulence Structure, In Proc. of 4th Symp. On Turbulent Shear Flows, Karlsruhe (1983), pp. 6.14-6.19.
3. Kristoffersen, R. and Andersson, H. I., Direct Simulations Of Low Reynolds-Number Turbulent Flow In A Rotating Channel, J. Fluid Mech., Vol. 256, (1993), pp. 163-197.
4. Andersson, H. I. and Kristoffersen, R., Turbulence Statistics of Rotating Channel Flow, In the Proc. Of 9th Symp. On Turbulent Shear Flows, (1993), Kyoto, Japan, pp. 53-70.
5. Oberlack, M., Cabot, W. and Rogers, M. M., Turbulent Channel Flow with Streamwise Rotation; Lie Group Analysis, DNS and Modelling. In the 1st int. Symp. in Turbulence and Shear Flow Phenomena, Santa Barbara, USA, (1999), pp. 85-90.
6. Iida, O. and Kasagi, N., Direct Numerical Simulation Of Unstably Stratified Turbulent Channel Flow, Journal Of Heat Transfer, Feb., Vol. 119, (1997), pp. 53-61.
7. Kasagi, N. and Ohtsubo, Y., Direct Numerical Simulation of Low Prandtl Number Thermal Field in a Turbulent Channel Flow, in Durst, F. et al (ed.), Turbulent Shear Flow 8, (1989), Springer, Berlin.
8. Kawamura, H., Ohsaka, K., Abe, H., and Yamamoto, K., DNS of Turbulent Heat Transfer in Channel Flow with Low to Medium-High Prandtl Number, Int. J. Heat Fluid Flow, Vol. 19, (1998) pp. 482-491.
9. Nishimura, M. and Kasagi, N. Direct Numerical Simulation of Combined and Natural Turbulent Convection in a Rotating Plane Channel, Proc. Of 3rd KSME-JSME, Thermal Engineering Conference, (1996), Korea, Vol. 3, pp. 77-82.
10. Kasagi, N., and Iida, O., Progress in Direct Numerical Simulation of Turbulent Heat Transfer, in the Proc. of the 5th ASME/JSME Joint Thermal Engineering Conference, (1999), pp. 1-17, San Diego, USA.